Scientia Iranica B (2022) 29(2), 461–477

Sharif University of Technology
Scientia Iranica
Transactions B: Mechanical Engineering
http://scientiairanica.sharif.edu

Prediction of work-roll failure in the hot ring rolling process

A. Negahban Boron[a,*], A. Maracy[b], M. Livani[a], and S.M. Nikouei[a]

a. *Faculty of Aerospace Engineering, Shahid Sattari Aeronautical University of Science and Technology, Tehran, Iran.*
b. *Department of Mechanical and Aerospace Engineering, Malek-Ashtar University of Technology, Shahinshahr, Esfahan, Iran.*

Received 4 July 2020; received in revised form 21 May 2021; accepted 13 September 2021

KEYWORDS
Ring rolling;
Thermo-mechanical stress;
Script code;
Stress life method;
ABAQUS.

Abstract. Work rolls in the hot ring rolling process are susceptible to various damages due to the contact with hot metal. Thermo-mechanical fatigue is one of these damages. In order to predict failure resulting from the thermo-mechanical stress in the work rolls, the developed code in ABAQUS was used. A comparison between three- and two-dimensional models was made and also, thermal and thermo-mechanical responses of work rolls with variable boundary conditions were investigated. The results demonstrated that by applying mechanical and thermal loads separately or simultaneously, the response of work rolls is completely different. In the mandrel, the location of the maximum equivalent stress is on the surface, while the location of equivalent maximum stress is on the subsurface of the main roll. Upon utilizing cumulative damage rules and the stress-life method, the thermo-mechanical fatigue life was estimated. The cumulated damage to the surface of the mandrel was higher than that to subsurface regions. In contrast to the mandrel, the cumulated damage to the subsurface of the main roll was higher than that to the surface regions. In hot ring rolling machines, these locations are prone to crack initiation as a result of the thermo-mechanical fatigue of the work rolls.

1. Introduction

Thermo-mechanical fatigue is one of the damages affecting the life of work rolls in hot rolling machines. It is a process in which crack propagation and initiation occur in critical positions exposed to simultaneous thermal and mechanical strain.

Up to now, numerous researches have investigated the hot rolling machines from different angles and using various approaches. For example, the rolling of various metals and metal composites has been investigated [1,2]. Some other studies could be related to either the effects of rolling on mechanical and metallurgical properties of the work piece [3–5] or controlling and optimizing the rolling conditions [6,7]. Another interesting aspect of rolling that has been studied is the prediction of the thermo-mechanical response of work rolls in various situations to evaluate the service life of work rolls. Song et al. [8] employed finite-element software and developed a thermo-mechanical coupling model to form ring-shaped IN-718. By using the model, they calculated the work-roll surface temperature, ring temperature, and the required loads for rolling. Shahani et al. [9] studied the effect of different process parameters on hot rolling of AA5083 aluminum alloy by making use of Finite Element Method (FEM). Harrer et al. [10] investigated the failure in silicon nitride rings for hot rolling and suitable conditions for making highly alloyed steel and super alloy wires. Based on FEM models and various assumptions, the thermal and

*. *Corresponding author.*
E-mail address: A-negahban@ssau.ac.ir (A. Negahban Boron)

doi: 10.24200/sci.2021.56341.4672

mechanical responses of strip and work rolls during a hot strip rolling have been investigated [11,12]. Yadav et al. [13] presented an approximate method to estimate temperature distributions in the work roll and strip in a rolling process. Benasciutti et al. [14] investigated a work roll in the hot flat rolling process by introducing a one-dimensional harmonic element and calculated the thermo-mechanical stresses in the work roll more rapidly than their previous works. Koohbor [15] developed an integrated mathematical model to study the thermo-mechanical behavior of strips and work rolls during the warm rolling process of steels. The model was first employed to solve the thermo-mechanical response of the rolled strip under steady-state conditions and then, used to apply proper boundary conditions for solving the thermo-mechanical response of the work roll. Deng et al. [16] studied the thermal and oxidation behaviors of a High-Speed Steel (HSS) work roll during hot flat rolling in actual service conditions. The effect of various parameters on temperature and thermal stress distributions within the work-roll was examined. Weidlich et al. [17] analyzed the effect of operational parameters of a hot rolling mill in the degradation process of a roll surface by thermal fatigue. They presented a new coefficient to predict the thermal damage to work rolls. Hanoglu and Sarler [18] simulated the hot rolling of various sections by means of meshless method. Palit et al. [19] tested progressive failure of a work roll in a hot strip mill. The results showed that in a work roll, crack initiation took place in subsurface and spalling occurred due to propagation of a circumferential crack through the shell. Hadizadeh et al. [20] inspected failure of repair welded continuous casting rolls by making changes to the microstructure. In the hot rolling process, Tolcha et al. [21] investigated creep-fatigue interaction damage. Their model consisted of three parts: mechanism of creep-fatigue interaction, elliptical crack growth rate, and H13 tool material response. The ABAQUS software was used for the finite element simulations.

By considering the literature review, it is clear that the most recent studies on the thermo-mechanical analysis of work rolls have focused on the flat rolling, and a few works have been conducted in the ring rolling process. Of note, the analysis and simulation of work rolls in a rolling machine are often time-consuming procedures owing to the rotation of work rolls and the variations of the boundary conditions during the process. Rotation of work rolls makes the finite element matrices changed and updated in every increment. To reduce the computational cost of simulation, the work rolls temperature and related thermal stress field are usually analyzed by researchers. Furthermore, it is evident that evaluation of thermo-mechanical analysis has been rarely taken into consideration.

Figure 1 shows the schematic of a radial-axial ring rolling machine and a flat rolling machine. Ring rolling is a rolling machine in which precise and seamless circularly-shaped metal parts are progressively forged. The mandrel, which is idle, moves to the main roll. The main roll is fixed and driven at a constant angular velocity. The axial rolls control the height of ring. The guide rolls guarantee that the ring remains circular during the process. In flat rolling, the plate passes through one or more pairs of work rolls to reduce the thickness.

As given in Figure 1, estimation of thermo-mechanical stresses in the work rolls of a ring rolling machine is rather different from a flat rolling. A brief comparison between the flat rolling and ring rolling is as follows: In the flat rolling, due to the symmetry of work rolls, it is common to analyze one of them, while in the ring rolling the diameter, applied loads and boundary conditions of work rolls are different and the symmetry assumption is not valid. In the ring rolling process, the contact surface between the ring and work rolls is time dependent. During the process, the ring's contact surface with the mandrel decreases and it increases with the main-roll while the contact surface in the flat rolling is constant. This feature of the ring rolling makes the applied forces and moments time dependent, which will affect the thermo-mechanical stresses. In the ring rolling, the

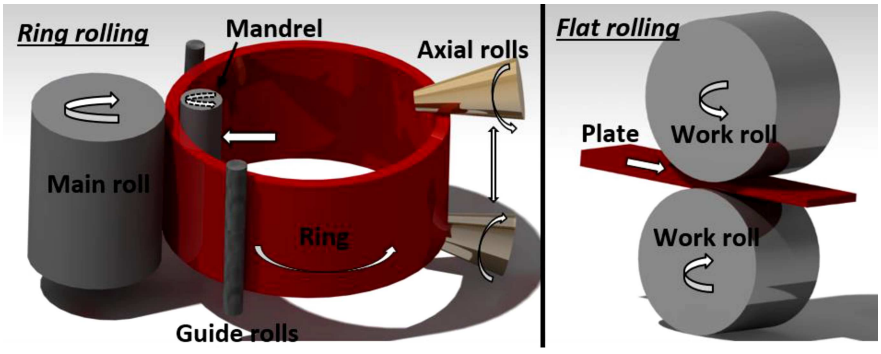

Figure 1. Schematic of a ring rolling machine and a flat rolling machine.

temperature-dependent thermo-mechanical properties of the metal can be different because of repeated rolling and variation of temperature in the ring and work rolls. In order to evaluate the process more accurately, the temperature-dependent thermo-mechanical properties of the metal (density, heat transfer coefficients, specific heat, work hardening, etc.) should be taken into account. To conclude, it is clear that the ring rolling process is time-dependent. At each moment, the work rolls and the ring are in a specific condition that makes their analysis too complicated. In the current research, upon developing a scripting code in the ABAQUS, the magnitude of thermal and mechanical loads is extracted, computed, and applied to work rolls simultaneously and all the time; besides, temperature-dependent properties are taken into account.

2. Applying boundary conditions in FEM

Work rolls in the rolling machines are simultaneously influenced by mechanical and thermal stresses. The thermal stress results from the non-homogeneous temperature distribution on the work roll which is caused by being in contact with the hot metal and the coolant. The mechanical stress results from the rolling pressure and contact with supporting work rolls. Thermo-mechanical stresses on the work rolls cause elastic and plastic strains that yield erosion, spalling, and unexpected damages. To reduce the computational time and simplify the model, the ring is considered as a hollow cylinder with the thickness and radius being time dependent during the process. The shape of the main work roll and mandrel is also cylindrical; thus, the general equation of heat transfer in cylinder coordinates is valid for them. The equations of thermo-elasticity could be obtained from kinematic relation, equations of motion, energy-scale equation, and constitutive equations [22]. The finite element formulation of a problem by making use of Galerkin weighted residual method is obtained in a standard way [23].

$$\left(\int_{V^e}\rho N_l N_m dV\right)\ddot{U}_{mi}+\left(\int_{V^e}G\frac{\partial N_l}{\partial x_j}\frac{\partial N_m}{\partial x_j}dV\right)U_{mi}$$
$$+\left(\int_{V^e}G\frac{\partial N_l}{\partial x_j}\frac{\partial N_m}{\partial x_i}dV\right)U_{mj}+\left(\int_{V^e}\lambda\frac{\partial N_l}{\partial x_i}\frac{\partial N_m}{\partial x_j}dV\right)$$
$$-\left(\int_{V^e}\beta\frac{\partial N_l}{\partial x_i}N_m dV\right)\theta_m=\int_{V^e}\rho F_i N_l dV+\int_{A^e}t_i N_l dA$$
$$l,m=1,2,...,n \qquad i,j=1,2,3. \tag{1}$$

$$\left(\int_{V^e}k\frac{\partial N_l}{\partial x_i}\frac{\partial N_m}{\partial x_i}dV\right)\theta_m-\left(\int_{V^e}T_0\beta\frac{\partial N_m}{\partial x_i}N_l dV\right)\dot{U}_{mi}$$
$$+\left(\int_{V^e}\rho c N_m N_l dV\right)\dot{\theta}_m=\int_{V^e}\rho R N_l dV-\int_{A^e}(\vec{q}.\vec{n})N_l dA$$
$$l,m=1,2,...,r \qquad i,j=1,2,3. \tag{2}$$

The finite element approximation of the equation of motion is expressed by Eq. (1) and the finite element approximation of the coupled energy equation is defined by Eq. (2). The general form of Eqs. (1) and (2) could be as follows:

$$[M]\{a\}+[C]\{v\}+[K]\{d\}=\{F\}. \tag{3}$$

As can be seen in Eq. (3), if the speed and acceleration of the elements are ignored, some terms in matrices will be ignored and the amount of computation time will be reduced. So, the strategy is to rotate the boundary condition around the work rolls and the work rolls should be fixed. This assumption reduces the effective matrices in the finite element model. The boundary conditions required for the simulation procedure can be considered according to Figure 2 as follows:

$$-k_r\frac{\partial T}{\partial r}\bigg|_{r=R_{1or2}}=h^*(T_{coolant}-T_{rollsurf})$$
$$+\eta\Lambda\sigma_B\left(T^4{}_{ambient}-T^4{}_{rollsurf}\right),$$
$$\left\{\begin{array}{ll}\eta=0 & T_{roll-initial}=30^\circ C\\ \eta=1 & T_{roll-initial}=500^\circ C\end{array}\right\}, \tag{4}$$

$$-k_r\frac{\partial T}{\partial r}|_{r=R_{1or2}}=h_c C(T_{ring}-T_{rollsurf})$$
$$C=C_1 \text{ or } C_2, \tag{5}$$

$$-k_r\frac{\partial T}{\partial r}|_{r=0.5R_{1or2}}=0, \tag{6}$$

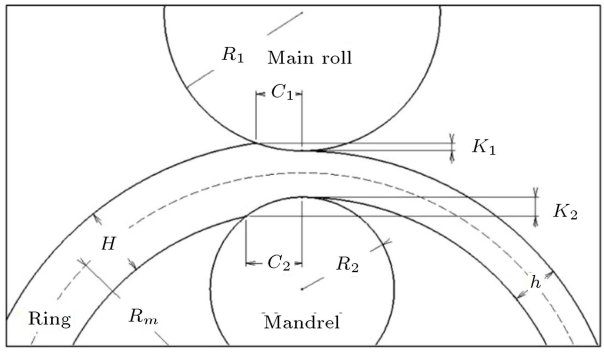

Figure 2. Schematic of the radial ring rolling and the related definitions.

$$p_{contact-zone} = \frac{F}{C.t} \qquad C = C_1 \text{ or } C_2, \tag{7}$$

$$u_i\Big|_{r=0} = 0, \tag{8}$$

where h^* is the convective heat transfer coefficient with different values in each region (air, water, or oil cooling region) except deformation zone. h_c is a property indicating the thermal conductivity between two bodies in contact. The radiation heat transfer is considered when the initial work-roll temperature is at 500°C. σ_B is Stefan-Boltzmann constant and Λ is radiative coefficient.

According to the non-symmetric and variable contact surface, the length of contact surface (C_1 and C_2) can be estimated by the research of Forouzan et al. [24]. The time-dependent contact area during the simulation is calculated using the above-mentioned values.

3. Estimation of work-roll's temperature with local cooling

The estimation of the surface temperature in a rolling process is of particular importance. Given these values, the rate of cooling and the material and service life of the work roll can be predicted. In a flat rolling, researchers usually use the plane strain assumption that has acceptable result. This assumption must be used carefully in a ring rolling process because the strain in the axial direction could not be neglected. Negahban et al. [25] studied the assumption of plane strain in the ring rolling and proposed a suitable range for using this assumption. As demonstrated by the results, if the values of distribution ratio of feed amount [26] and mandrel's velocity be small enough (less than 1 and 0.5 mm/s), the results of 2D simulations have good agreement with the three-dimensional simulation.

3.1. Flat rolling

ABAQUS software has the film and D-flux subroutines for thermal analysis. These subroutines can be used to define a non-uniform film coefficient or heat flux as a function of position, time, temperature, etc. in heat transfer analysis [27]. Therefore, thermal stress analysis needs another time-consuming simulation to convert this temperature field history to stress field. In order to conquer this problem and save time, a script python code was developed. Two separate simulations were employed to compare the results of the explicit and implicit algorithms. There is an important balance between the efficiency of an explicit algorithms based on lumped matrices and the accuracy of an implicit algorithm with consistent matrices. The lumped matrix approach has clear advantages in computational efficiency, but with some loss of accuracy. In problems where high accuracy of temperature distribution is required, the use of the more accurate through more expensive consistent matrix is justified [28]. It should be noted that both methods have a critical time step to avoid spurious oscillations (implicit) or divergence (explicit).

The proposed modeling procedure contains several sub-models in which boundary conditions are changed. In these models, the cooling and heating zones are rotated in the reversed direction by the script code. In every step, the surface elements located on this zone are selected and the proper boundary conditions are imposed; then, a simple transient thermo-mechanical analysis is simulated. Each time step is equal to one degree of work roll's rotation. The research conducted by Benasciutti et al. [14] was used in order to simulate the local cooling and estimate the temperature field on the work roll. The work-roll FE model has a fine mesh, with a total of 10800 elements and 11161 nodes. The outer surface is divided into 360 segments. The radial partitions are divided by seed 30 and bias 15. The four-node linear element (CPE4RT) is used.

The results have been obtained and variations in the node temperature on the surface of the work roll are shown in Figure 3. The same temperature trend has been predicted by the models. In other words, the surface's temperature rises rapidly in the heating zone. When roll surface leaves this zone, the surface's temperature decreases with a specific trend. In the cooling zone, the surface's temperature decreases rapidly; so, there is a cusp at the point where the cooling zone begins. When the roll leaves this zone, the surface's temperature rises slowly. This is due to the heat transfer from the internal nodes to external nodes.

In the heating zone where the pick point occurred, the first model (implicit algorithm) predicted the temperature to be greater than Benasciutti results. The second model (explicit algorithm) predicted the temperature to be lower than Benasciutti results. In other locations, the predicted temperature, in general,

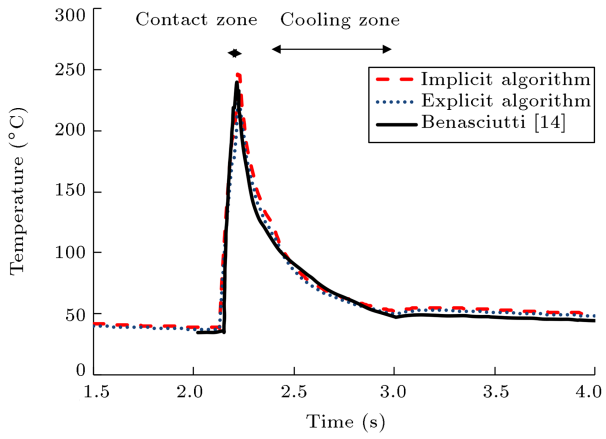

Figure 3. Comparison of surface temperature in different models.

is higher (max 10%). The comparison between the models prepared by script code indicates that simulation time is almost the same. The simulation time using a personal computer (Intel core i7- 4790 3.5 GHz, RAM-16 G) took about 10 hours. This thermal stress simulation of the work rolls by Benasciutti took 13 days [29] and in other work with a 1D parametric element, which allows for the analysis of plane axisymmetric structures [14], it required 5 hours.

The advantages of the proposed developed code in Abaqus and modeling procedure can simulate 2D and 3D geometries without any simplification and also, simultaneously simulate thermal and mechanical analyses. The other advantages are the ability to impose the mechanical and thermal loads history and variable contact surfaces into a model. With respect to simulation results, the implicit method was used to evaluate thermo-mechanical stress in the ring rolling process.

3.2. Ring rolling

As mentioned before, the simulation of the model using the typical software environment is not feasible. Therefore, the model and the steps with the variable boundary conditions are prepared by the script code. Each time step is equal to one degree of the work roll's rotation. According to the history of loading and temperature, at each step, the initial and boundary conditions on the work roll are computed and added to the model. In other words, in each step, the boundary conditions such as rolling force, area of heating and cooling zones, etc. are changed. At the end of each step, the results are extracted and used as an initial state condition for the subsequent sub-model. Figure 4 shows a schematic of the work roll's modeling with a partial boundary condition and the algorithm used in the models. The α, γ, and β represent the angle of the heating zone, the angle of cooling zone, and the angle between two zones, respectively.

In order to apply thermal flux at each step, the current contact length and temperature of the work roll and ring in the previous step are required. Upon using the developed code in ABAQUS, these values are obtained from the previous step and the empirical data [8], respectively. For the simulation, the models are constructed with Python code in ABAQUS. The dimensions and conditions are in accordance with the information, as provided in Table 1.

According to the low velocity of work rolls and small deformations in the ring, the assumption of the plane strain in the present simulation is acceptable [25]. In order to reduce the computational cost, it is possible to isolate and analyze work rolls individually. As mentioned before, the general strategy in this research is that instead of analyzing a work roll under different boundary conditions caused by its rotation, the boundary conditions rotate around the work roll. By doing this, a simple transient thermo-mechanical problem is solved in each step. Hence, the volume of effective matrices in the governing equation in finite element formulation can be reduced.

As three-dimensional thermo-mechanical simulation of the ring rolling needs a huge computational cost, the thermal analysis with variable boundary conditions was carried out. The results of the simulation are shown in Figure 5 where the temperature variation of the four different points on the work rolls' surface is shown. The initial temperature of the work rolls is 30°C. Variation in the temperature on the work rolls surface depends on the location in the axial direction. At every rotation of the work roll, the graphs indicate that the maximum temperature occurs in the contact zone. Point 1 is located on the axial symmetry plane of the work roll. It is clear that the temperature at the symmetry plane of the work roll is maximum. Due to the symmetry plane at point 1, the two-dimensional heat transfer occurs. At point 2, there is no symmetry and the heat flux is transmitted in three directions. Therefore, the work roll's surface temperature is slightly lower. At points 3 and 4 where the ring and the work roll are not in contact, the temperature drop increases further to reach the initial temperature of work rolls.

As mentioned, in the three-dimensional model,

Table 1. Dimensions and conditions of the ring rolling process.

Work rolls' material	H-13 tool steel	Feed rate (mm/s)	0.33
Ring material	Ti6Al4V	Colling sector (deg)	90
Outer radius of mandrel (mm)	60	Colling zone	30–120
Inner radius of mandrel (mm)	30	Initial rolls temperature (°C)	30 or 500
Outer radius of main-roll (mm)	200	Friction coefficient	0.5
Inner radius of main-roll (mm)	100	Emissivity coefficient	0.8
Outer radius of ring (mm)	120	Environment temperature (°C)	30
Inner radius of ring (mm)	80	Air convection coefficient (W/(m^2.°C))	50
Height of rolls (mm)	200	Coolant convection coefficient (W/(m^2.°C)) -water	10100
Height of the contact area (mm)	160	Coolant convection coefficient (W/(m^2.°C))- oil	1000
Angular velocity of main-roll (rad/s)	6.28	Contact heat conductivity (W/(m^2.°C))	10000

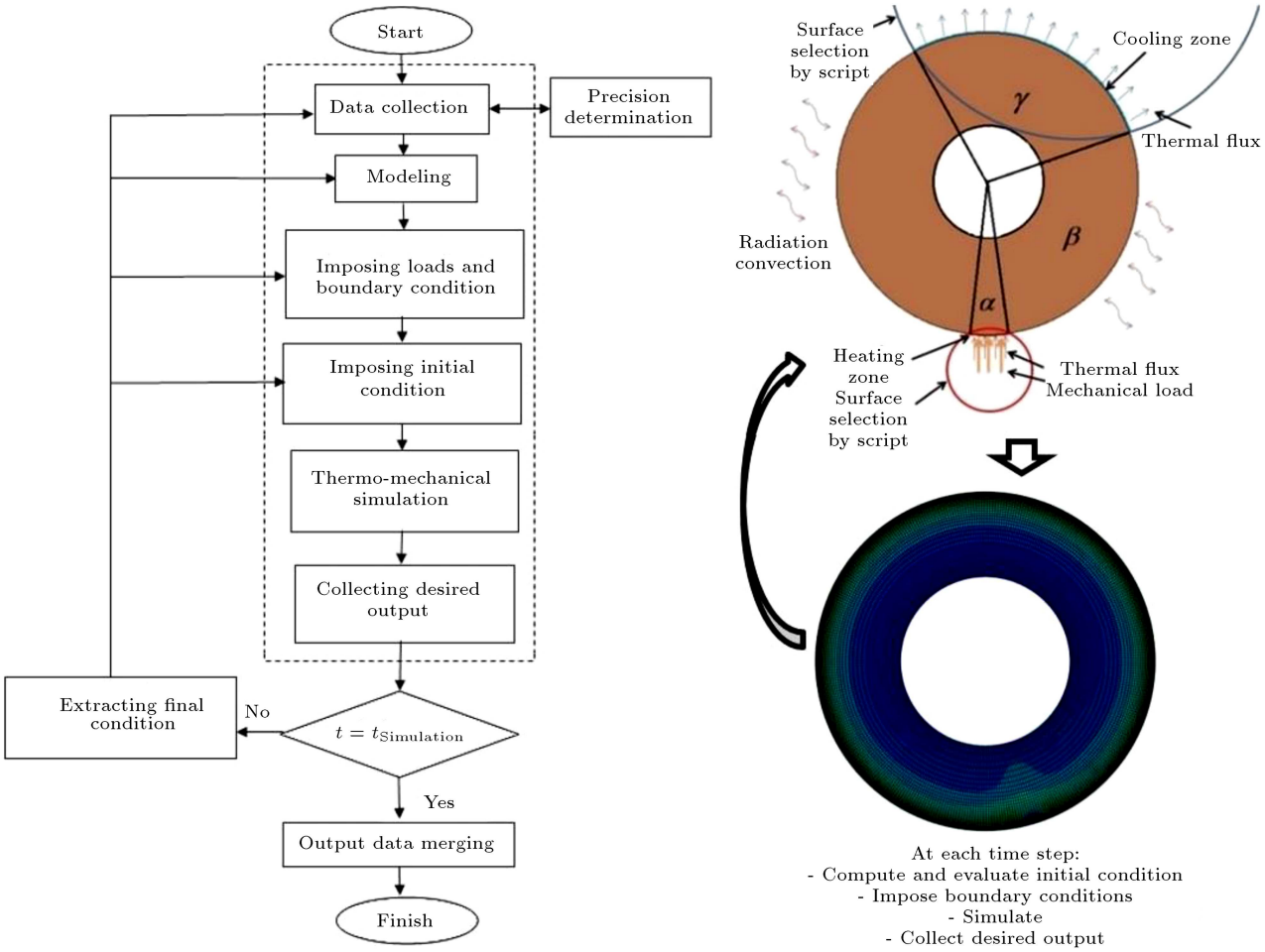

Figure 4. Flowchart and schematic of work-roll modeling with a partial boundary condition.

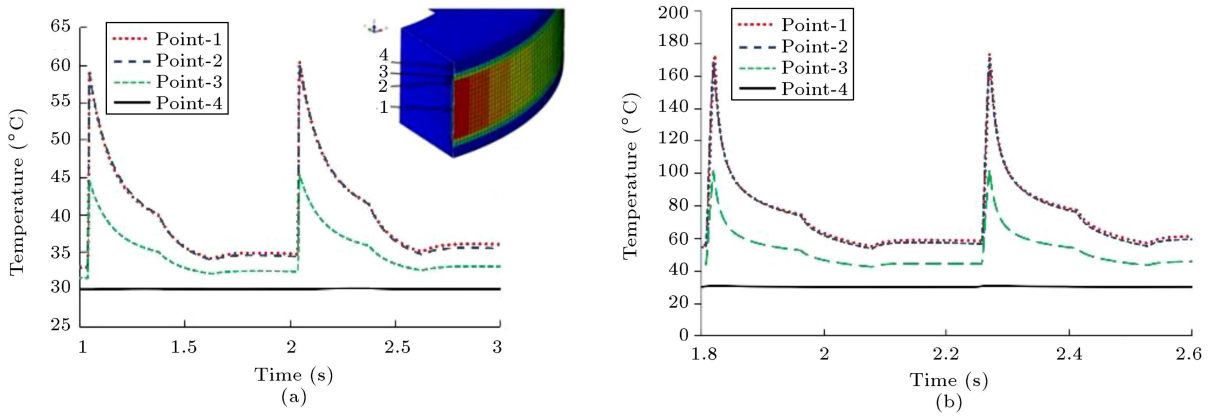

Figure 5. Variation of temperature in the three-dimensional simulation of work rolls: (a) Main roll and (b) Mandrel.

maximum temperature occurs at the symmetry plane. To compare the temperature in two-dimensional and three-dimensional models, the temperature variation on the symmetry plane of the 3D model was compared with the two-dimensional model.

Figure 6 makes a comparison between two- and three-dimensional simulations. As can be clearly seen, the two-dimensional model predicts a higher temperature than the three-dimensional one in the contact zone. In other locations, there is no significant difference between the models. In the three-dimensional model, the thermal flux which is transmitted from the ring to the main roll spreads in three directions. In the two-dimensional model, the same thermal flux enters the work-roll, but the thermal flux is transmitted in two directions. This issue causes the nodes to exhibit a

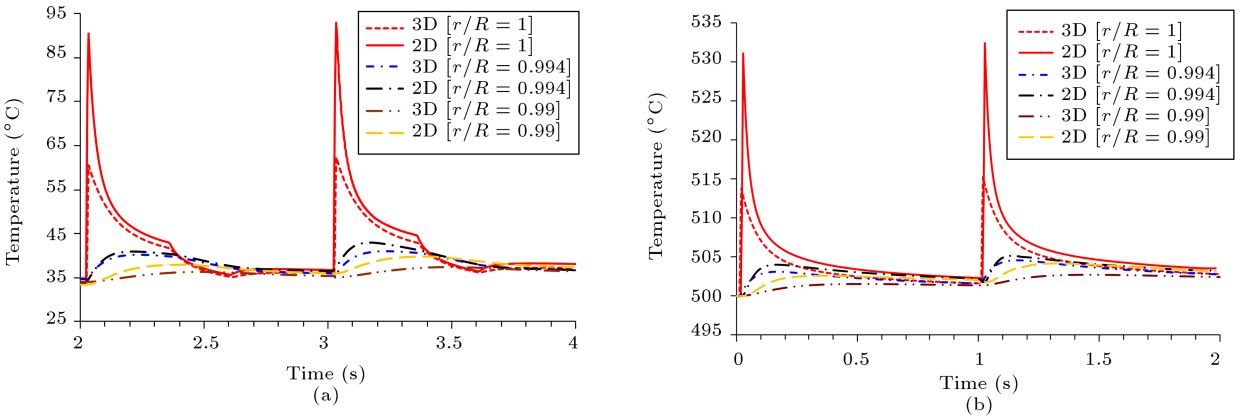

Figure 6. Variation of temperature in 3D and 2D simulations: (a) Initial temperature of 30°C and (b) Initial temperature of 500°C.

higher temperature rise in the two-dimensional model. According to Figure 6(a), the temperature of the main roll surface sharply increases and reaches its maximum in the contact region. By leaving this area, the temperature decreases by a specific rate to enter the forced convection zone (cooling zone). In this area, the temperature decline is higher and causes a cusp in the temperature profile. As the work-roll surface passes through this area due to a greater reduction in the temperature of the surface nodes compared to internal nodes, heat flux transfers from the inside to the outside of the work roll and the surface's temperature increases. The temperature of coolant is constant during the process, but during the process, the temperature of the internal surfaces increases. This leads to an increase in temperature difference between the inner and surface elements. In each rotation of the work roll, the mentioned condition is met. As a result, the total work-roll temperature experiences a minor increase at each rotation. Figure 6(b) illustrates the situation in which the initial temperature of the main roll is 500°C and no cooling is performed on the surface. In this case, as mentioned earlier, the heat transfer of the work roll is done by radiation and convection with the surrounding environment. Figure 6(a) shows that on the contact surface, the surface's temperature of the work roll increases rapidly and decreases with a specific rate after leaving the area. In this case, there is no sudden change in boundary conditions on the work roll surface except the contact area; no cusp in the temperature profile is observed.

According to these figures, when the temperature of the main roll is 30°C; temperature increases in the contact surface in two- and three-dimensional models are about 170% and 70%, respectively. Each rotation of the work roll causes 8% and 4% average increases in the temperature of the surface in two- and three-dimensional models, respectively. When the work roll's temperature is 500°C, the thermal flux entering the work roll is reduced due to a decrease in the temperature difference. In this case, the rises of the temperature in the contact area in the two- and three-dimensional models are about 6% and 3%, respectively, and each rotation provides the work roll surface with lower than 1% increase in temperature.

In the study conducted by Sonboli and Serajzadeh [11], the two-dimensional finite element model indicates higher temperature in the contact region compared to the measured value. Considering the results of their work and this research, in general, the prediction of temperature is higher in the two-dimensional model. Therefore, the 2D model predicts greater thermal stresses in the work rolls.

4. Estimation of thermo-mechanical stresses

In this study, by making use of ABAQUS software and the developed code, mechanical and thermal loads are simultaneously applied to the work rolls and thermo-mechanical stresses are calculated. By doing this, computational cost declines dramatically and the accuracy of the results is higher.

As mentioned earlier, in order to investigate the thermo-mechanical stress and estimate the life of work rolls in the ring rolling process, two initial temperatures have been considered. In the first case, the work roll's temperature is at 30°C. In this case, in order to avoid temperature's rise in the work roll and prolong its life, its surface is cooled down by water. This increases the life of the work roll. In another case, the work roll's temperature is at 500°C to avoid the chilling effect in the ring. In this case, the local cooling is not applied to the work roll, and the work roll transfers heat to the ambient by convection and radiation. The model is prepared based on the plane strain assumption according to Table 1. The heat load at each step is determined according to the ring's temperature at any moment. The value of the forces generated by the rolling process is derived from separate dynamic analysis and the history of the force applied to the work

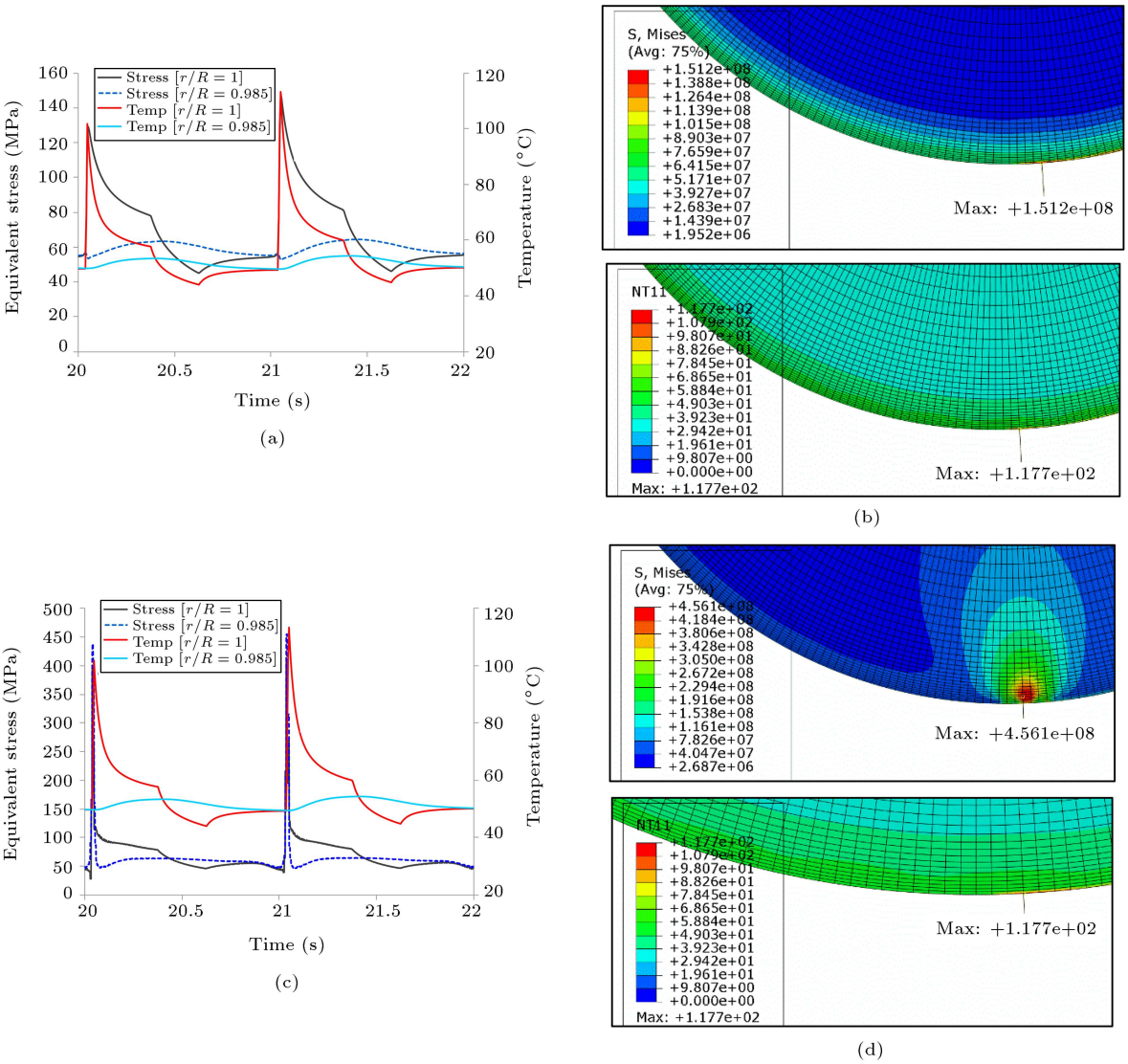

Figure 7. Variation of temperature and equivalent stress in the main roll (initial temperature of 30°C: (a) History of thermal stress and temperature in an element's integration point, (b) temperature and thermal stress field at the 22nd second of simulation, (c) history of thermo-mechanical stress and temperature in an element's integration point, and (d) temperature and thermo-mechanical stress field at the 22nd second of simulation (S = Von-Mises equivalent stress, NT = Nodal Temperature).

roll is listed in Table 2. The magnitude of pressure load on each work roll is estimated by the contact length and load history at any moment.

The values of temperature and stress in the main roll in the case where only the thermal loads are applied are given in Figure 7(a). According to this figure, it can be observed that the predominant variations of temperature occur on the main roll surface and the lower surfaces experience less temperature variations. Severe changes in temperature and maximum temperature lead to higher thermal stresses on the surface. The maximum temperature and thermal stress variations occur on the main roll surface in the contact area. This has been reported by various researchers in the hot rolling process. The magnitude of temperature and the

Table 2. Load history applied to the work roll.

Time (s)	Force (N)
0	955001
3.00	1.20E+06
6.00	1.27E+06
9.00	1.30E+06
12.50	1.37E+06
15.50	1.45E+06
18.50	1.49E+06
22.00	1.65E+06
25.50	1.70E+06

thermal stress field at the 22nd second of simulation are shown in Figure 7(b). If only the heat load is applied to the main roll, critical conditions occur on the surface of the work roll. By applying mechanical and thermal loads on the main roll (Figure 7(c)), similar to the previous case, the most significant temperature changes occur on the work roll surface; however, the location of the Maximum Equivalent Stress (MES) is transferred from the surface to the lower in the contact area (Figure 7(d)). In another area, the obtained stresses are almost equal to the case where only heat loads are applied.

The values of the plane strain stress's components in the radial direction along the work roll with a temperature of 30°C are given in Figure 8. Upon applying the mechanical forces, normal stresses on the surface reach the maximum value. However, the maximum shear stress occurs in the sub-surface. According to the relation of the equivalent Von-Mises stresses, it is obvious that the increase in shear stresses below the surface has a significant effect on the equivalent Von-Mises stress and makes this stress reach its maximum value below the surface. This phenomenon can be justified by the stress caused by the contact known as the Hertzian stresses. Under the surface, due to increase in the Von-Mises stress, there is a possibility of crack initiation and propagation to the surface.

The variation of temperature and stress on the mandrel by applying thermal and thermo-mechanical loads at normalized distances of 1 and 0.86 are given in Figure 9. If the mechanical load is applied to the mandrel, the MES occurs at the normalized distance $r/R = 0.86$. According to this figure, it is evident that the temperature's rise in the mandrel is more than the main roll. Therefore, the magnitude of thermal stress is higher than that in the main roll. The variation of thermal stress on the internal surface is negligible. However, because of a rise in temperature in the mandrel in the forming process, the value of thermal stress increased. This graph shows that the trends of thermal stress and temperature are the same. Upon applying thermal and mechanical loads on the mandrel simultaneously in contrast to the main roll, the

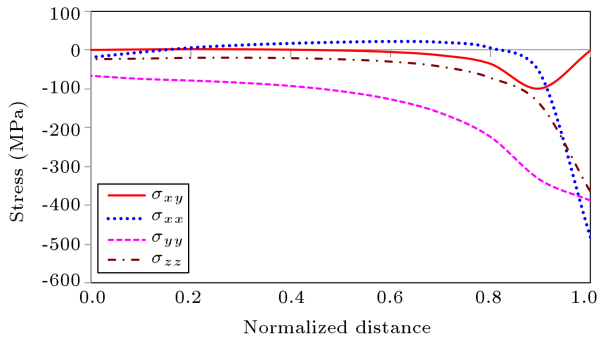

Figure 8. Variation of shear and normal stresses at the radial normalized distance of the work-roll.

MES occurs on the surface of the mandrel. The results of simulation show that the thermal loads have greater effects than mechanical loads on the mandrel. The mechanical load tending to the MES takes place under the mandrel surface; on the other hand, the thermal load tending to the MES takes place on the surface. These phenomena resulted in the hydrostatic pressure increase in the mandrel. Therefore, the amounts of thermo-mechanical Von-Misses stresses are less than thermal stresses on the surface of the mandrel (Figure 9(b)). The magnitude of temperature and thermo-mechanical stress field at the 22nd second of simulation are shown in Figure 7(c).

Overall, these opposing trends in the work rolls indicate that the value and location of maximum thermo-mechanical stresses are completely different. The response of the mandrel to thermo-mechanical load is similar to work rolls in a hot flat rolling.

Figure 10 shows the history of the main-roll's Von Mises stress at an element's integration point on the surface and a subsurface element with a ratio of $(r/R = 0.985)$. Figure 10(a) and (b) are related to the main roll with initial temperatures of 30°C and 500°C, respectively. It is evident from these figures that during the process, with the increase of mechanical load, Von Mises stress increases. The value of equivalent stress below the surface is on average 50% higher than that on the surface. The mechanical forces in the contact area have a significant effect on the equivalent Von Mises stress, and the rest of the regions are affected by thermal loads. In Figure 10(b), due to the absence of cooling on the work roll's surface, there is no cusp in the thermo-mechanical stress.

Figure 11(a) shows a history of the mandrel's Von Mises stress at an integration point on the surface and a subsurface element with a ratio of $(r/R = 0.86)$ at a temperature of 30°C. The figure depicts that the trend of thermo-mechanical stress in the mandrel differs from that in the main roll. The consequent effect of the temperature rise in the mandrel is shifting the location of MES. At the early stage, maximum thermo-mechanical stress occurs on the subsurface that is related to the mechanical load. During the process and greater heat transfer to the mandrel, the thermal stress overcomes the mechanical stress and the location of MES shifts to the surface. The mandrel with the initial temperature of 500°C has been simulated to investigate the effect of work-roll initial temperature on thermo-mechanical stress. The history of the Von Mises stress at an integration point on the mandrel surface and below it $(r/R = 0.86)$ is shown in Figure 11(b). From this figure, it is obvious that without cooling practice on the mandrel, the value of mean stress increases gradually. These figures also depict that the magnitude of the amplitude stress decreases slightly and remains almost steady during the process. In another research, effects

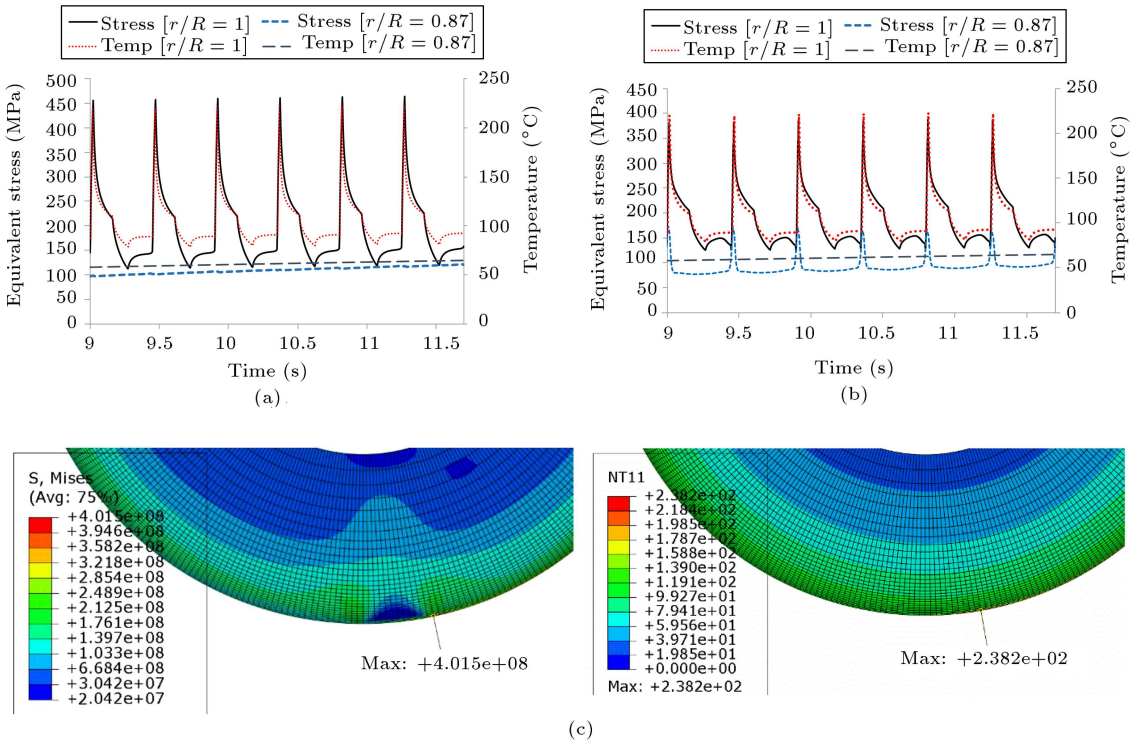

Figure 9. Variation of temperature and equivalent stress in the mandrel (initial temperature of 30°C): (a) History of thermal stress and temperature in an element's integration point, (b) history of thermo-mechanical stress and temperature in an element's integration point, and (c) temperature and thermo-mechanical stress field at the 22nd second of simulation (S = Von-Mises equivalent stress, NT = Nodal Temperature).

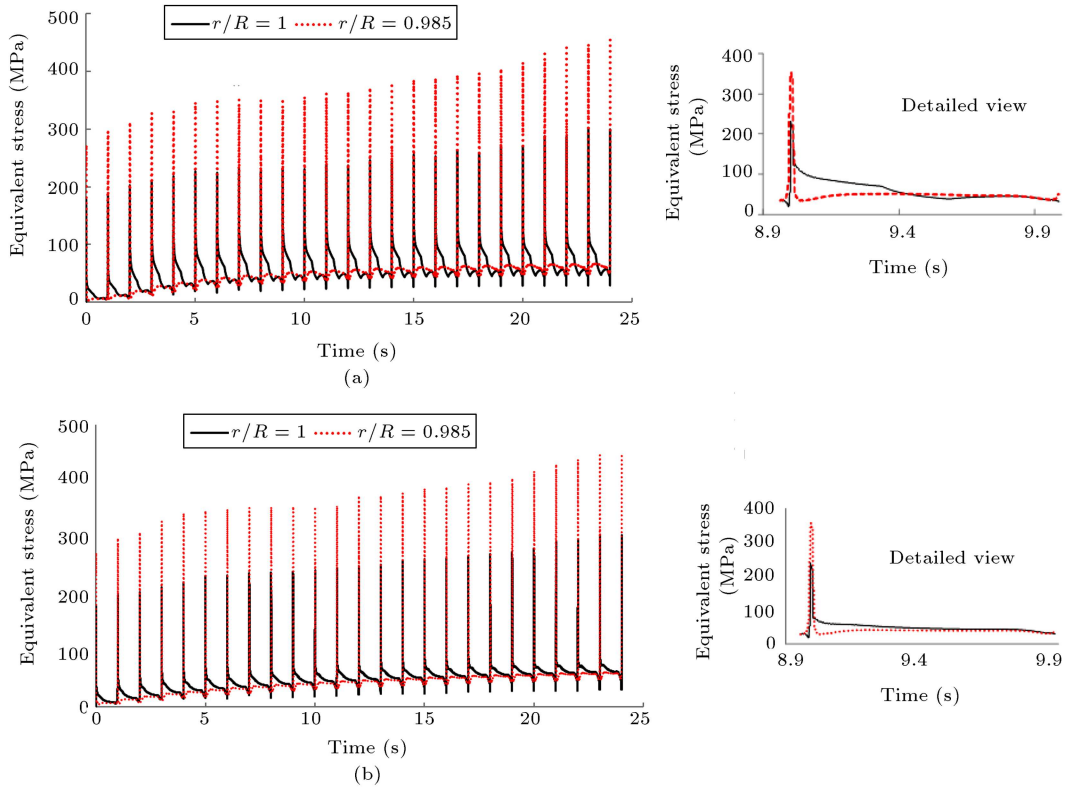

Figure 10. History of thermo-mechanical Von-Mises stress in the main roll: (a) Initial temperature of 30°C and (b) initial temperature of 500°C.

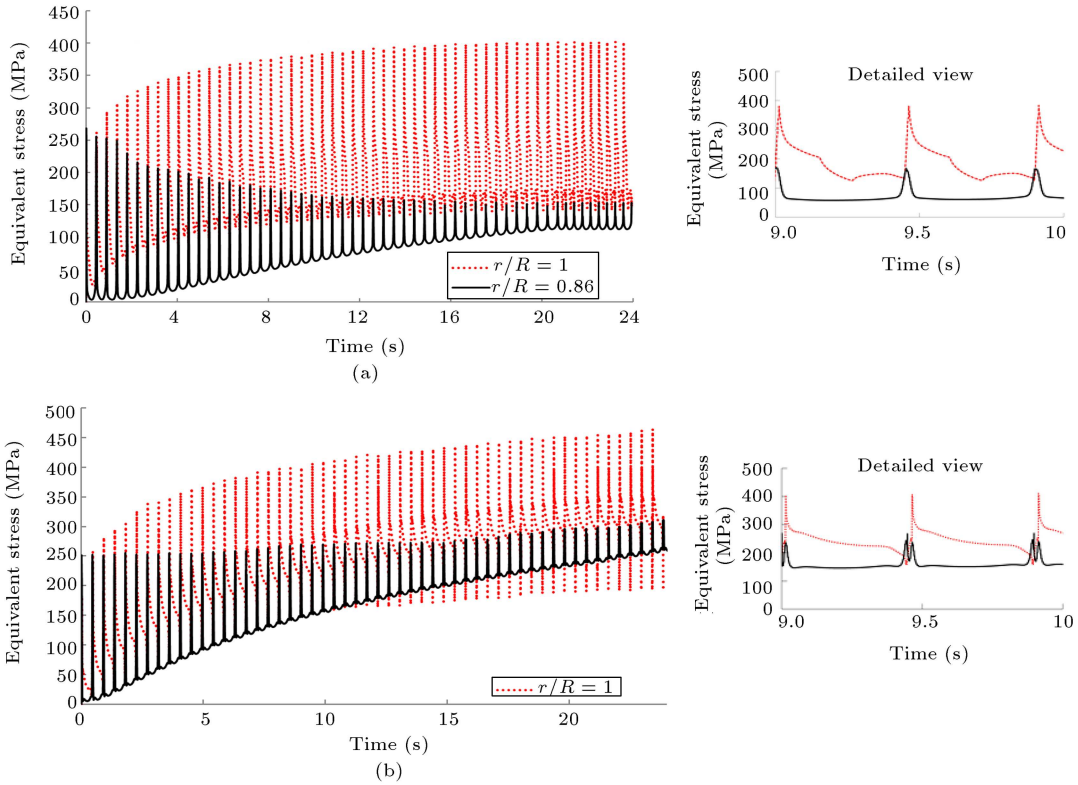

Figure 11. History of Von Mises stress in the mandrel: (a) Initial temperature of 30°C and (b) initial temperature of 500°C.

of different initial temperatures and cooling practice on the thermo-mechanical stress were investigated [30]. As can be demonstrated by the results, to reduce the thermal stresses, it is necessary to maintain the initial temperature of the work roll as far as possible with proper cooling. Proper cooling minimizes the amount of thermo-mechanical stresses and the heterogeneous temperature field in the work roll.

A cycle equals 24 seconds of loading history; therefore, it is the time that the ring needs to form completely. It is assumed that the delay time between the forming processes of rings is long enough for the work rolls to return to their initial condition. Therefore, this history is considered as a loading block. During a cycle, the Von Mises stress in the contact region of the work rolls suddenly changes. This change results from the mechanical and thermal loads. As the work rolls pass this region, the equivalent stress experiences a sudden and significant drop. This phenomenon is related to the absence of mechanical loads and conduction heat transfer. In non-contact regions, thermal stresses have a greater effect on thermo-mechanical stresses. For example, in the main roll, the equivalent stress on the surface is higher than that on the inner surfaces because of higher temperature on the surface. In the subsurface elements, the heat transfer is delayed; therefore, this heat flux does not have a sudden effect on the value of stress.

5. Estimation of thermo-mechanical fatigue life

Stress-based methods are among the oldest approaches to estimating life that have become conventional since the mid-nineteenth century and they are also known as $S-N$ method. In the cases where cyclic stresses are significant parameters and plastic deformations are insignificant in the parts, stress-based methods have acceptable accuracy in the life of more than $10^3 - 10^4$ cycles [31]. The work rolls are made of H-13 alloy and its thermo-mechanical properties are according to the references [32–34]. If required, the curve, which was fitted based on experimental values, was used for some thermo-mechanical properties. Proper correction coefficients and thermo-mechanical properties are shown in Table 3.

The standard $S-N$ diagram for this alloy which is produced by the Electroslag Remelting (ESR) method and heat treatment in $R = -1$ is extracted using the research conducted by Philip on this alloy [35]. By applying suitable coefficients and considering the geometry, production method, and work-roll temperature, the stress-life diagram is prepared for the desired working conditions. The standard and modified $S-N$ curves are shown in Figure 12.

According to Figures 10 and 11, the stresses are within the range of high cycle fatigue. Each block has specific destructive effect; thus, the cumu-

Table 3. Work-roll correction coefficients and thermo-mechanical properties.

Work rolls' materials	H-13 tool steel
Elastic module (GPa)	186
Ultimate tensile strength (MPa)	$\begin{cases} 1625(30^\circ C) \\ 1200(500^\circ C) \end{cases}$
Yield tensile strength (MPa)	$\begin{cases} 1350(30^\circ C) \\ 985(500^\circ C) \end{cases}$
Poisson coefficient	0.285
Initial rolls temperature (°C)	30–500
Specific heat (j/(kg.°C))	460
Density (kg/m^3)	7840
Thermal conductivity as a function of temperature (W/(m.°C))	$k = 10^{-7} \cdot T^3 - 10^{-4} \cdot T^2 + 5.78 \cdot 10^{-2} \cdot T + 16.131$
Thermal expansion as a function of temperature ($10^{-5}/^\circ C$)	$\alpha = 3 \cdot 10^{-7} \cdot T^2 - 10^{-4} \cdot T + 1.0971$
Flow stress as a function of plastic strain (MPa)	$\sigma_p = -268.72 \cdot {\varepsilon_p}^6 + 1795.5 \cdot {\varepsilon_p}^5 - 4676.9 \cdot {\varepsilon_p}^4 + 5995 \cdot {\varepsilon_p}^3 - 3943.2 \cdot {\varepsilon_p}^2 + 1334.7 \cdot \varepsilon_p + 693.05$
Surface treatment factor	0.84
Reliability correction factor	0.753
Temperature correction factor (500°C)	0.768

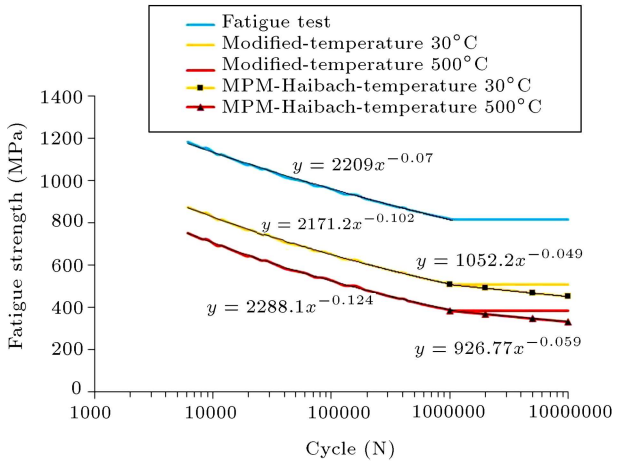

Figure 12. Standard and modified $S-N$ curves.

lative damage hypotheses are employed to estimate the damage caused by each load in the block. In the present research, the cumulative damage hypotheses include the Palmgren-Miner [36] modified Palmgren-Miner (Haibach) [37], and Manson-Halford [38] methods. In these methods, it is assumed that the failure occurs when the sum of damage reaches a specific value. This relationship is as follows:

$$\sum \frac{n_i}{N_{fi}} = D_{PM}, \tag{9}$$

where n_i and N_{fi} are the number of loading and fatigue life in a specific range of stresses, respectively. D_{PM} is the critical value of damage. If the critical value of damage reaches 1, the work piece will fail. However, it has been determined that the value of this coefficient varies for materials and alloys. Haibach [39] offered a value of 0.3 for steels. The value of N_{fi} is estimated by making use of $S-N$ curve. The theories of Palmgren-Miner, Haibach, and Manson-Halford are summarized in Table 4. As mentioned before, most of the amplitudes and mean stresses are below the fatigue limit; therefore, the Haibach rule is suitable. On the other hand, Manson-Halford is used for load-sequence effect.

S_a, S_e, N, n, N_D, $n_{i,eq}$, N_{ref}, and k are stress amplitude, endurance limit, number of cycles until failure at a specified stress level, number of loading cycles at a given stress level, number of cycles at the deflection point, equivalent damage cycles, shortest life levels, and slope factor of $S-N$ curve, respectively [38,40]. In each block, the value of equivalent mean and alternating stresses will be determined. Eq. (9) changes in the following to estimate the number of blocks until failure:

$$\sum n_b \left(\frac{n_i}{N_{fi}}\right) = D_{PM}, \tag{10}$$

where n_b is the number of loading blocks until failure.

There are several methods for estimating the limited life and the effect of mean stress on fatigue life. To estimate the effect of mean stress, the Goodman, Morrow, and Gerber methods are chosen. According to the loading history, the value of fatigue safety factor is assumed to be 1.5. By making use of the modified $S-N$ curves, the damage caused by each loading cycle on and below the surface was examined.

The estimated damages by Palmgren-Miner linear damage accumulative rule in the MES location in the main roll and mandrel at an initial temperature of 30°C in the first block with Goodman, Morrow, and Gerber methods are zero. This value indicates that Palmgren-Miner method predicts infinite life for the work rolls.

The estimated damages by the modified Palmgren-Miner(Haibach) linear damage accumulative

Table 4. Summary of cumulative damage rules.

$\begin{cases} S_a \geq S_e & N_i = N_D.\left(\frac{S_a}{S_e}\right)^k \\ S_a < S_e & N_i \to \infty \end{cases}$	$D = \sum n_i/N_i$	Palmgren-Miner
$\begin{cases} S_a \geq S_e & N_i = N_D.\left(\frac{S_a}{S_e}\right)^k \\ S_a < S_e & N_i = N_D.\left(\frac{S_a}{S_e}\right)^{2k-1} \end{cases}$	$D = \sum n_i/N_i$	Modified Palmgren-Miner-Haibach (MPM-Haibach)
$D_1 = \frac{n_1}{N_1}, \quad n_{i,eq} = N_i.[D_{i-1}]^{\left(\frac{N_{ref}}{Ni}\right)^{0.4}}$ $D_i = \left[\frac{n_{i,eq}+n_i}{N_i}\right]^{\left[\frac{N_i}{N_{ref}}\right]^{0.4}}$		Manson-Halford

rule in the main roll (initial temperature 30°C) with Goodman, Morrow, and Gerber methods in the first block are 2.83E-08, 4.67E-09, 1.47E-10, respectively. These values in the mandrel are 1.34E-10, 1.77E-11, and 1.27E-13, respectively. It should be underlined that Goodman relation predicted a higher equivalent fully reversed stress amplitude. Therefore, the relative damage is higher than the other mentioned relations. Furthermore, the equivalent fully reversed stress amplitude computed by Gerber relation is less than that by Morrow relation. The one block's cumulative damage in the work rolls shows that the damage to the mandrel is less than that to the main roll. The numbers of tolerable blocks can be predicted by adding the cumulative damage in each block to reach a critical value.

The estimated damage by the Manson-Halford-Haibach power damage accumulative rule in the main roll (initial temperature 30°C) with various methods in the first block is 1.27E-08, 2.04E-09, 5.98E-11, respectively. The estimated damages in the mandrel by this rule are 3.67E-11, 4.67E-12, and 1.13E-13, respectively. In the first block, the results show that the magnitude of damage by Manson-Halford-Haibach rule is lower than that by previous linear damage rules. It is notable that the computed damage at the end of the process becomes higher than previous rules. This rule considers the effect of loading sequence and gradually predicts higher damage in the subsequent loading history. Therefore, the predicted tolerable blocks are less than other rules. The numbers of tolerable blocks by means of the mentioned methods and rules are summarized and shown in Table 5.

The estimated damages by the Palmgren-Miner linear damage accumulative rule in the MES location in the main roll at an initial temperature of 500°C in the first block with Goodman, Morrow, and Gerber methods are 2.29E-05, 2.87E-06, and zero, respectively. These values in the case of mandrel are 5.66E-06 and zero. The initial impression from the computed damages is that the higher initial temperature of the work rolls reduces the strength of material and leads to higher damage. The estimated damages by the modified Palmgren-Miner (Haibach) linear damage accumulative rule in the main roll (initial temperature of 500° C) using different methods in the first block are 2.79E-05, 5.60E-06, and 4.19E-07, respectively. These values in the mandrel are 1.52E-05, 1.23E-07, and 6.34E-10, respectively. The estimated damage by Manson-Halford-Haibach power damage accumulative rule in the main roll (initial temperature 500°C) with different methods in the first block is 8.37E-06, 2.12E-

Table 5. Work roll's life estimation at different temperatures.

Life estimation method		Modified Palmgren-Miner-Haibach		Manson-Halfod-Haibach	
		n_b (500°C)	n_b (30°C)	n_b (500°C)	n_b (30°C)
Goodman	Main-roll ($r/R = 0.98$)	9462	>1E7	10727	>1E7
	Mandrel ($r/R = 1$)	14530	>1E7	19707	>1E7
Morrow	Main-roll ($r/R = 0.98$)	45700	>1E7	53600	>1E7
	Mandrel ($r/R = 1$)	2113432	>1E7	2429680	>1E7
Gerber	Main-roll ($r/R = 0.98$)	609433	>1E7	717703	>1E7
	Mandrel ($r/R = 1$)	>1E7	>1E7	>1E7	>1E7

06, and 1.56E-07, respectively. The estimated damages in the mandrel by this method are 3.66E-06, 1.97E-08, and 1.79E-10, respectively.

With respect to the value of the predicted damages in the work rolls, it is clear that the value of damage to the mandrel is less than the main roll. Also, it is evident that the life of the subsurface elements is far less than that of the surface elements in the main roll, and vice versa in the mandrel. This causes the initiation of cracks to occur below the main roll surface, which moves continuously to the surface of the work roll. This causes sudden failure due to thermo-mechanical stresses in the main roll. On the other hand, in the mandrel, the initiation of cracks related to thermo-mechanical stress occurs on the surface.

As mentioned before, the main roll is mostly affected by the mechanical stress and the mandrel affected by thermal stress. By making use of cooling practice on the surface of the work roll, the amount of mean thermal stress in the work roll and cumulative damage decreases. For increasing life of work rolls at an initial temperature of 500°C, it is necessary to apply cooling practice to work rolls. However, it has no considerable effect on reducing the thermo-mechanical stresses in the main roll.

In the mandrel, with an initial temperature of 500°C and cooling its surface by oil with the same temperature, the estimated damage by the modified Palmgren-Miner (Haibach) in the MES location in the first block with Goodman, Morrow, and Gerber methods is 1.69E-06, 5.90E-08, and 4.29E-10, respectively. The estimated damage by Manson-Halford-Haibach with the mentioned methods in the first block is 4.74E-07, 1.35E-08, and 7.34E-10, respectively. Through the oil cooling of mandrel, an average reduction of 60% is achieved in the amount of the cumulative damage.

As mentioned before, the amount of cumulative damage in the first loading block with Haibach rule is higher than that with Manson-Halford rule. However, in the Manson-Halford rule, the cumulative damage in each block rises rapidly. Therefore, the predicted number of tolerable blocks with this method is less than that with the Haibach method. In the mentioned rules, when the total damage with respect to the alloy reaches 0.3, it is expected that the work roll fails. The results are shown in Table 5.

6. Conclusion

In this research, two- and three-dimensional simulations of the hot ring rolling process were compared. The thermo-mechanical response of work rolls with variable boundary conditions was studied by making use of the developed code in ABAQUS software. In the following, the effect of thermo-mechanical stresses on the life of the work rolls in the hot ring rolling process was investigated. Usually, the damages caused by corrosion, oxidation, wear, etc. have destructive effects on the surface and the damage caused by them can be observed with regular inspections. The results indicated that the effect of thermo-mechanical stresses on fatigue life could not be easily observed. The results of the research can be summarized briefly as follows:

- The plane strain and three-dimensional simulation of the ring rolling process provided approximately the same temperature prediction if it was carried out in the mentioned allowed range. Overall, the plane strain simulation predicted higher temperature values;
- The simulation of the hot ring rolling process by applying thermal or thermo-mechanical loads offered completely different results;
- Thermal stresses had a greater effect on the surface of the work roll. The extreme temperature variations occurred in this region. On the subsurface, change in thermal stress was reduced due to less temperature variations;
- Mechanical stresses had a greater effect on subsurface of the work roll. Upon applying mechanical forces on the surface of the work roll, the Von-Mises stress reached the maximum value in the subsurface, being in agreement with the Hertzian stress theory;
- The response of the main roll to thermo-mechanical stresses in the hot ring rolling was the same as that of work rolls in the cold flat rolling. In contrast, the response of the mandrel was mostly the same as that of work rolls in the hot flat rolling;
- The predicted life on the subsurface of the main roll was much less than that on the surface of the work roll. This caused the initiation and propagation of cracks in the subsurface. It led to sudden failure by thermo-mechanical fatigue;
- Thermal stresses had a greater effect on the mandrel. By appropriate cooling practice on the surface of the work roll, the amount of service life considerably increased. The results showed that the failure in the mandrel due to thermo-mechanical stress occurred on the mandrel surface.

Nomenclature

a	Generalized acceleration vector
C	Generalized damping matrix
$C_{1,2}$	Length of contact zone
c	Specific heat per unit mass
D	Critical value of damage
d	Generalized displacement vector
F_i	External force per unit mass

F	External force vectors
G	Shear modulus
h^*	Convective heat transfer coefficient
h_c	Contact thermal conductivity coefficient
K	Generalized stiffness matrix
k	Coefficient of thermal conductivity
	Slope factor of $S-N$ curve
M	Generalized mass matrix
N_D	Number of cycles at the deflection point
N_{ref}	Shortest life of life levels
$N_{l,m}$	Shape function
N	Number of cycles until failure at a specified stress level
$n_{i,eq}$	Equivalent damage cycles
n_b	Number of loading blocks until the failure
n	Number of loading cycles at a given stress level
q	Heat flux per unit area
R	Strength of the internal heat source per unit mass
r	Total number of nodal points
S_a	Stress amplitude
S_e	Endurance limit
T_0	Initial temperature
t_i	Prescribed traction component on the boundary surface
u_i	Displacement vector with respect to coordinate (i)
ν	Generalized velocity vector
α	Coefficient of thermal expansion
β	Thermoelastic constant
θ	Temperature difference
λ	Lame elastic constant
Λ	Radiative coefficient
ρ	Mass density
σ_B	Stefan-Boltzmann constant
ε_p	Flow stress
ε_p	Plastic strain

References

1. Wang, M., Sheng, J., Wang, L.-D., Yang, Z.-Y., Shi, Z.-D., Wang, X.-J., and Fei, W.-D. "Hot rolling behavior of graphene/Cu composites", *J. Alloys Compd.*, **816**, p. 153204 (2020).
2. Gu, B., Chekhonin, P., Schaarschuch, R., Oertel, C.-G., Xin, S.W., Ma, C.L., Zhou, L., Gan, W.M., and Skrotzki, W., "Microstructure, texture and hardness of a metastable β-titanium alloy after bar-rolling and annealing", *J. Alloys Compd.*, **825**, p. 154082 (2020).
3. Deng, G.Y., Tieu, A.K., Su, L.H., Zhu, H.T., Reid, M., Zhu, Q., and Kong, C. "Microstructural study and residual stress measurement of a hot rolling work-roll material during isothermal oxidation", *Int. J. Adv. Manuf. Technol.*, **102**(5–8), pp. 2107–2118 (2019).
4. Masoudi Nejad, R., Shariati, M., Farhangdoost, K., and Atrian, A. "Rolling contact fatigue analysis of rails under the influence of residual stresses induced by manufacturing", *Sci. Iran.*, **26**(3), pp. 1427–1437 (2019).
5. Qaban, A., Mohmed, T., Quazi, M.M., and Naher, S. "The effect of Al and Nb contents, cooling rate and rolling condition on the microstructure and corrosion behaviour of HSLA steel", *Mater. Today Commun.*, **25**, p. 101362 (2020).
6. Hu, Z., Wei, Z., Sun, H., Yang, J., and Wei, L. "Optimization of metal rolling control using soft computing approaches: a review", *Arch. Comput. Methods Eng.*, pp. 1–17 (2019).
7. Goryany, V., Schubrikoff, E., and Myronova, O. "Roll optimization via numerical modeling of stress distribution", *Mater. Test.*, **62**(1), pp. 35–39 (2020).
8. Song, J.L., Dowson, A.L., Jacobs, M.H., Brooks, J., and Beden, I. "Coupled thermo-mechanical finite-element modelling of hot ring rolling process", *J. Mater. Process. Technol.*, **121**(2–3), pp. 332–340 (2002).
9. Shahani, A.R., Nodamaie, S.A., and Salehinia, I. "Parametric study of hot rolling process by the finite element method", *Sci. Iran.*, **16**(2 B), pp. 130–139 (2009).
10. Harrer, W., Morrell, R., Lengauer, M., Danzer, R., Berroth, K., and Zleppnig, W. "Failure analysis of silicon nitride rings for hot rolling of highly alloyed steel and superalloy wires", *Eng. Fail. Anal.*, **18**(1), pp. 138–147 (2011).
11. Sonboli, A. and Serajzadeh, S. "A model for evaluating thermo-mechanical stresses within work-rolls in hot-strip rolling", *J. Eng. Math.*, **72**(1), pp. 73–85 (2012).
12. Sayadi, H. and Serajzadeh, S. "Prediction of thermal responses in continuous hot strip rolling processes", *Prod. Eng.*, **9**(1), pp. 79–86 (2014).
13. Yadav, V., Dixit, U.S., and Singh, A.K. "An approximate method for computing the temperature distributions in roll and strip during rolling process", *Proc. Inst. Mech. Eng. Part B J. Eng. Manuf.*, **228**(9), pp. 1118–1130 (2014).
14. Benasciutti, D., De Bona, F., and Munteanu, M.G. "A harmonic one-dimensional element for non-linear thermo-mechanical analysis of axisymmetric structures under asymmetric loads: The case of hot strip rolling", *J. Strain Anal. Eng. Des.*, **51**(7), pp. 518–531 (2016).

15. Koohbor, B. "Finite element modeling of thermal and mechanical stresses in work-rolls of warm strip rolling process", *Proc. Inst. Mech. Eng. Part B J. Eng. Manuf.*, **230**(6), pp. 1076–1086 (2016).

16. Deng, G.Y., Zhu, Q., Tieu, K., Zhu, H.T., Reid, M., Saleh, A.A., Su, L.H., Ta, T.D., Zhang, J., and Lu, C. "Evolution of microstructure, temperature and stress in a high speed steel work-roll during hot rolling: Experiment and modelling", *J. Mater. Process. Technol.*, **240**, pp. 200–208 (2017).

17. Weidlich, F., Braga, A.P.V., da Silva, L.G.D.B., Júnior, M.B., and Souza, R.M. "The influence of rolling mill process parameters on roll thermal fatigue", *Int. J. Adv. Manuf. Technol.*, **102**(5–8), pp. 2159–2171 (2019).

18. Hanoglu, U. and Šarler, B. "Hot rolling simulation system for steel based on advanced meshless solution", *Metals (Basel).*, **9**(7), p. 788 (2019).

19. Palit, P., Patel, S.N., Mathur, J., and Shenoy, S. "Analysis of a progressive failure of a work-roll in hot strip mill", *J. Fail. Anal. Prev.*, **19**(5), pp. 1297–1303 (2019).

20. Hadizadeh, B., Bahrami, A., Eslami, A., Abdian, K., Araghi, M.Y., and Etezazi, M. "Establishing the cause of failure in continuous casting rolls", *Eng. Fail. Anal.*, **108**, p. 104346 (2020).

21. Tolcha, M.A., Altenbach, H., and Tibba, G.S. "Modeling creep-fatigue interaction damage and H13 tool steel material response for rolling die under hot milling", *Eng. Fract. Mech.*, **223**, p. 106770 (2020).

22. Balla, M. "Formulation of coupled problems of thermoelasticity by finite elements", *Period. Polytech. Mech. Eng.*, **33**(1–2), pp. 59–70 (1989).

23. Eslami, M.R., Hetnarski, R.B., Ignaczak, J., Noda, N., Sumi, N., and Tanigawa, Y., *Theory of Elasticity and Thermal Stresses*, Springer, **197**, pp. 727–733 (2013).

24. Forouzan, M.R., Salimi, M., and Gadala, M.S. "Three-dimensional FE analysis of ring rolling by employing thermal spokes method", *Int. J. Mech. Sci.*, **45**(12), pp. 1975–1998 (2003).

25. Negahban, A., Maracy, A., and Barati, E. "Investigation of 2-D hot ring rolling simulation and effects of different parameters on forming process of jet's spool", *J. Aeronaut. Eng.*, **18**(1), pp. 75–92 (2016).

26. Wang, M., Yang, H., Sun, Z.C., and Guo, L.G. "Analysis of coupled mechanical and thermal behaviors in hot rolling of large rings of titanium alloy using 3D dynamic explicit FEM", *Journal of Materials Processing Technology*, **209**(7), pp. 3384–3395 (2009).

27. Abaqus, V. "6.14 Documentation", *Dassault Syst. Simulia Corp.*, **651** (2014).

28. Huebner, K.H., Dewhirst, D.L., Smith, D.E., and Byrom, T.G., *The Finite Element Method for Engineers*, John Wiley & Sons (2008).

29. Benasciutti, D. "On thermal stress and fatigue life evaluation in work-rolls of hot rolling mill", *J. strain Anal.*, **47**(5), pp. 297–312 (2012).

30. Negahban, A., Barati, E., Maracy, A., and Vahdat azad, N., "Effect of initial temperature and cooling practice on thermo-mechanical stress of ring rolling", *Amirkabir J. Mech. Eng.*, **52**(8), pp. 21–30 (2019).

31. Shigley, J.E. and Mischke, C.R., *Mechanical Engineering Design: In SI Units*, McGraw-Hill (2005).

32. Benedyk, J.C. "Aerospace and high-performance alloys database", pp. 67–118, UNE 36072.2 (2008).

33. Yan, H., Qian, G., and Hu, Q. "Development of flow stress of AISI H13 die steel in hard machining", *J. Wuhan Univ. Technol. Sci. Ed.*, **22**(2), pp. 187–190 (2007).

34. eFunda Inc, *eFunda: The Ultimate Online Reference for Engineers* (2014).

35. Philip, T.V. "ESR: a means of improving transverse mechanical properties in tool and die steels", *Met. Technol.*, **2**(1), pp. 554–564 (1975).

36. Fatemi, A. and Yang, L. "Cumulative fatigue damage and life prediction theories: A survey of the state of the art for homogeneous materials", *Int. J. Fatigue*, **20**(1), pp. 9–34 (1998).

37. Haibach, E. "Modified linear damage accumulation hypothesis", *Proc. Conf. Fatigue Welded Struct*, pp. Xx–Xxii (1970).

38. Lee, Y.-L., Pan, J., Hathaway, R., and Barkey, M. *Fatigue Testing and Analysis: Theory and Practice*, Butterworth-Heinemann (2005).

39. Lee, Y.-L., Barkey, M.E., and Kang, H.-T., *Metal Fatigue Analysis Handbook: Practical Problem-Solving Techniques for Computer-Aided Engineering*, Elsevier (2011).

40. Köhler, M., Jenne, S., Pötter, K., and Zenner, H., *Load Assumption for Fatigue Design of Structures and Components*, Springer (2017).

Biographies

Ali Negahban Boron received his BS degree in Aerospace Engineering from Shahid Sattari Aeronautical University of Science and Technology, Tehran, Iran, 2005, his MS degree in Aerospace Engineering from Malek Ashtar University of Technology, Iran, 2008, and his PhD degree in Aerospace Engineering from Malek Ashtar University of Technology, Iran, 2018. He is currently an Assistant Professor at the School of Aerospace Engineering at the Shahid Sattari Aeronautical University of Science and Technology. His research activities include metal forming, composite structures, fatigue, and finite element analysis.

Abdolali Maracy is an Assistant Professor of Mechanical Engineering at the Malek-ashtar University of Technology, Iran. He received his PhD in Mechanical and Manufacturing Engineering from Birmingham University, England, 1992. His current research focuses on

ring rolling, forging, and extrusion processes.

Mostafa Livani received his BS degree in Aerospace Engineering from Shahid Sattari Aeronautical University of Science and Technology, Tehran, Iran, 2007, his MS degree in Aerospace Engineering from Sharif University of Technology, Tehran, Iran, 2009, and his PhD degree in Aerospace Engineering from Malek Ashtar University of Technology, Tehran, Iran, 2016. He is currently an Assistant Professor at the School of Aerospace Engineering at the Shahid Sattari Aeronautical University of Science and Technology. His research activities include smart material, FG and composite structures, dynamics, aeroelasticity, and creep.

Sayed Mohamad Nikouei received his BS degree in Aerospace Engineering from Shahid Sattari Aeronautical University of Science and Technology, Tehran, Iran, 2008 and his MS degree in Aerospace Engineering from Sharif University of Technology, Tehran, Iran, 2011. He is a PhD Candidate in Mechanical Engineering Amir Kabir University of Technology, Tehran, Iran, 2014. He is currently a lecturer at the School of Aerospace Engineering at the Shahid Sattari Aeronautical University of Science and Technology. His research activities include metal forming, machining, residual stress analysis, and 3D printers.